

HUG: Hierarchical Urban Gaussian Splatting with Block-Based Reconstruction for Large-Scale Aerial Scenes

Mai Su
Peking University
Beijing, China

Zhongtao Wang
Peking University
Beijing, China

Huishan Au
Peking University
Beijing, China

Yilong Li
Peking University
Beijing, China

Xizhe Cao
Peking University
Beijing, China

Chengwei Pan
Beihang University
Beijing, China

Yisong Chen
Peking University
Beijing, China

Guoping Wang
Peking University
Beijing, China

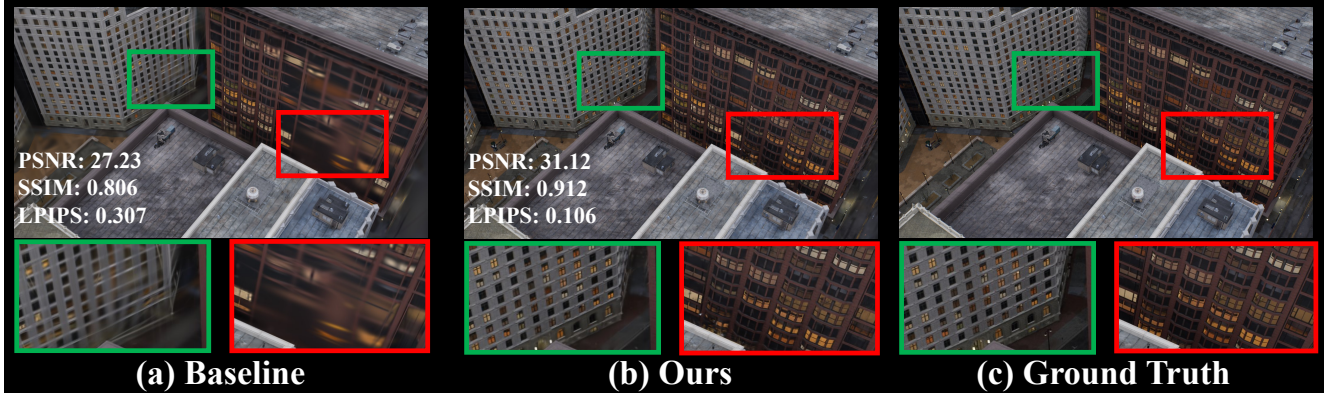


Figure 1. Our method achieves the SOTA performance on the *MatrixCity* dataset. In (a), we show the results of the best-performing baseline method, CityGS [17]. In (b), we present the results of our method, demonstrating clear improvements in visual quality. For reference, (c) displays the Ground Truth. The quantitative metrics for this view, shown in (a) and (b), underscore the superiority of our method in terms of reconstruction quality.

Abstract

3DGS is an emerging and increasingly popular technology in the field of novel view synthesis. Its highly realistic rendering quality and real-time rendering capabilities make it promising for various applications. However, when applied to large-scale aerial urban scenes, 3DGS methods suffer from issues such as excessive memory consumption, slow training times, prolonged partitioning processes, and significant degradation in rendering quality due to the increased data volume. To tackle these challenges, we introduce **HUG**, a novel approach that enhances data partitioning and reconstruction quality by leveraging a hierarchical neural Gaussian representation. We first propose a visibility-based data partitioning method that is sim-

ple yet highly efficient, significantly outperforming existing methods in speed. Then, we introduce a novel hierarchical weighted training approach, combined with other optimization strategies, to substantially improve reconstruction quality. Our method achieves state-of-the-art results on one synthetic dataset and four real-world datasets.

1. Introduction

With the increasing complexity of large urban 3D scenes and the growing demand for high-quality rendering, efficient scene reconstruction and rendering techniques have become critical. In recent years, Radiance Field Rendering methods, particularly those based on Neural Radiance Fields [20], have gained significant attention and es-

tablished themselves as the dominant paradigm for high-quality 3D scene reconstruction and rendering. More recently, 3D Gaussian Splatting [11] has emerged as a promising alternative, offering new possibilities for efficient scene representation. However, despite their effectiveness, these methods often face inefficiencies when dealing with large-scale scenes or intricate details. To address these challenges, we propose a novel approach named HUG for large-scale urban scene reconstruction and rendering that optimizes both the data partitioning process and the reconstruction pipeline, while incorporating an efficient Level of Detail (LOD) representation.

To reconstruct blocks of large urban scene, many existing methods train large redundant regions around the block boundaries to ensure boundary reconstruction accuracy, resulting in significant computational waste. In contrast, our approach begins with an enhanced block-based reconstruction pipeline that concentrates more on improving reconstruction quality within blocks. By reducing the need for redundant training regions and focusing more on the reconstruction quality within blocks, we release the waste of computing resources, particularly when processing complex or large-scale scenes, and enables improvements in reconstruction quality.

Building upon this foundation, we integrate a neural Gaussian representation with an efficient block-wise hierarchical LOD architecture. This combination ensures high-fidelity scene rendering with low computational cost, regardless of distance. By streamlining computational overhead and maintaining high rendering quality, we enable efficient representation of large-scale aerial scenes without compromising performance.

Finally, we demonstrate the effectiveness of our method by achieving State-of-the-Art (SOTA) results on five public benchmarks for large-scale aerial scenes.

Our contributions can be summarized as follows:

- We propose a simple and effective visibility-based partitioning strategy for large-scale aerial datasets, outperforms existing methods in speed, requiring about 1 minute to process each scene.
- We introduce a hierarchical neural Gaussian representation tailored for block-based reconstruction of large-scale aerial urban scenes. Our work also presents a novel hierarchical weighted image supervision strategy along with additional optimizations to further enhance reconstruction quality.
- Our method achieves state-of-the-art results on one synthetic and four real-world datasets, showcasing its advantage over existing approaches.

2. Related Work

2.1. Neural Rendering

Neural rendering, particularly through Neural Radiance Fields (NeRFs) [2, 3, 19, 20, 24, 25, 32, 34], has made significant strides in 3D scene reconstruction and novel view synthesis. NeRFs represent a scene as a continuous volumetric function, where a deep neural network is trained to map 3D coordinates and viewing directions to radiance and density values. This implicit representation, combined with volumetric rendering, yields highly realistic novel views. However, the method’s dependence on dense sampling and prolonged network inference times often leads to high computational costs and limits its rendering quality. To address this, several approaches have sought to accelerate NeRF-based rendering. Techniques such as InstantNGP [22] leverage multi-resolution hash grids and compact neural networks to achieve substantial speedups while maintaining high visual fidelity. Mip-NeRF 360 [3] extends NeRF’s capabilities to unbounded scenes while maintaining excellent anti-aliasing and high-quality rendering by properly handling multi-scale observations. Similarly, Plenoxels [8] uses sparse voxel grids to efficiently represent the scene’s continuous density field, delivering notable performance improvements.

Alongside NeRFs, point-based rendering has emerged as an alternative for faster scene rendering. 3D Gaussian Splatting (3DGS) [11] stands out by using 3D Gaussians as primitives, combining explicit geometry with rasterized rendering to enable real-time performance without sacrificing visual quality. Scaffold-GS [18] introduces a hierarchical structure to further improve scene reconstruction. By organizing Gaussians into a scaffold-like framework, this approach enables more accurate and efficient scene representations. Several works have focused on optimizing and compressing Gaussian representations [7, 21], offering inspiration for large-scale, high-quality scene reconstruction. Despite the promise of these works, challenges remain, particularly concerning storage cost when scaling to large scenes.

To tackle the issue of resource saturation, we propose a divide-and-conquer data partitioning strategy that decomposes the environment into manageable regions, ensuring more efficient allocation of computational resources during training. Additionally, we implement a Level-of-Detail system that efficiently adapts the scene’s complexity based on the viewer’s perspective.

2.2. Large Scale Scene Reconstruction

Large-scale scene reconstruction is a challenging problem that involves generating high-fidelity 3D models from extensive data sources. Early approaches [9, 13, 23] restore camera poses using the Structure from Motion (SfM)

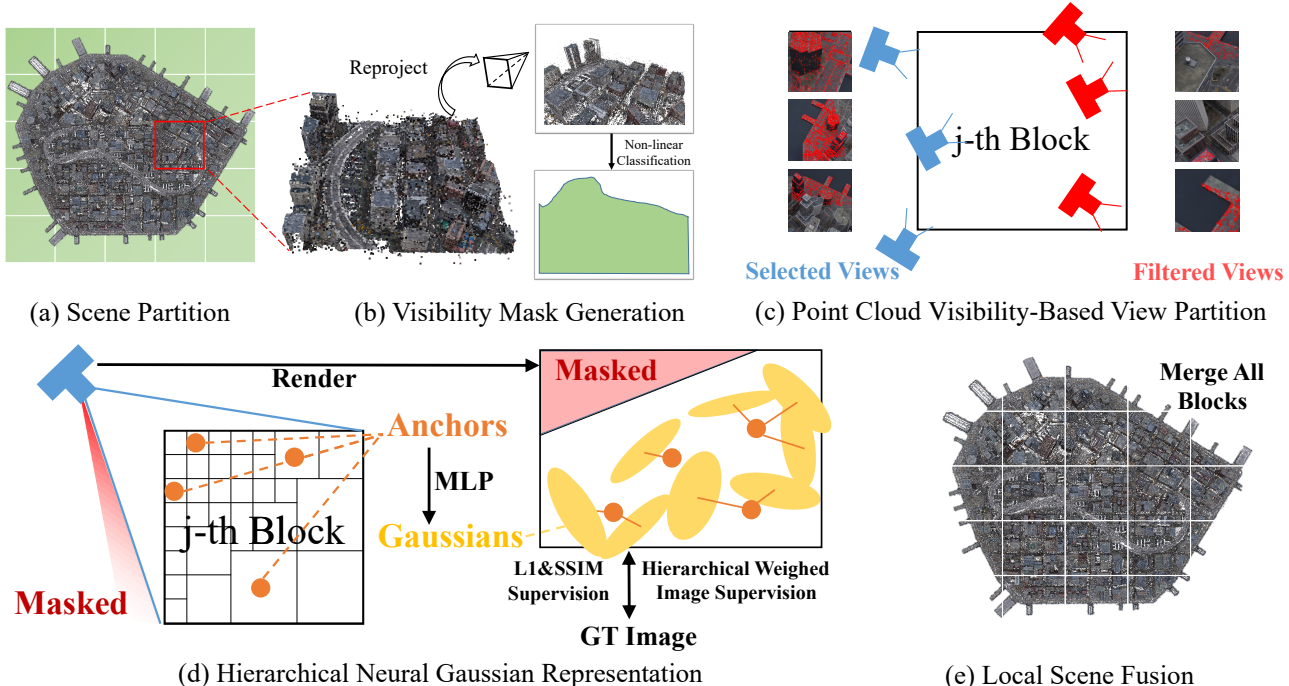


Figure 2. An overview of our proposed method, HUG. (a). The sparse point cloud from COLMAP [27] is used to uniformly partition the scene into blocks. (b). For each view, visibility masks for all blocks are generated by reprojecting 3D points within blocks into the image space and segmenting corresponding visible regions. (c). Views are assigned to training block j if the visible sparse point cloud exceeds a threshold. (d). During training each block, anchors within the view frustum are selected based on their position and level. These selected anchors infer the neural Gaussians used for rendering and are optimized using our hierarchical weighted image supervision along with other constraints. (e). All trained blocks are seamlessly merged and rendered.

method. Photo Tourism [28] and Building Rome in a Day [1] rely on large image datasets to generate precise 3D reconstructions. With the emergence of Neural Radiance Fields (NeRF) [20], the paradigm for large-scale scene reconstruction has shifted toward learning-based methods that synthesize photorealistic views of a scene from sparse or incomplete inputs. However, these techniques often face limitations in scaling to large, complex environments due to their high computational and storage demands. To address these issues, recent works such as BlockNeRF [31] and MegaNeRF [33] have employed divide-and-conquer strategies, partitioning scenes into smaller blocks and optimizing each independently, thereby reducing memory consumption. LesGo [6] combined LiDAR point clouds with 3DGS, achieving impressive modeling and rendering quality for large-scale garages. Some recent Gaussian-based approaches [5, 15, 17] also deploy similar strategies to divide large scenes into small blocks and rebuild them respectively. However, these methods train redundant regions around the block boundaries to avoid boundary artifacts, leading to significant computational waste.

Our method overcomes these inefficiencies by utilizing the visibility mask, allowing it to focus on the specific regions that require detailed reconstruction.

2.3. Level of Detail Scene Representation

The primary objective of Level-of-Detail (LOD) techniques is to balance computational efficiency with visual fidelity, reducing resource usage for distant or less critical objects while maintaining high-quality rendering. This is achieved by adjusting detail levels based on object proximity or relevance.

In the context of learning scene representations, incorporating LOD has become a significant area of active research. Early efforts like Mip-NeRF [2] and NGLoD [30] have utilized hierarchical representations and multi-resolution voxel grids to represent scenes at varying levels of detail. Unlike NeRF-based methods, the LOD handling in 3DGS scene representation is more intuitive. Several Gaussian-based methods [15, 17] achieve the LOD structure by merging the properties of Gaussian volumes after training all the scenes.

Inspired by Octree-GS [26], we use a framework that combines a hierarchical octree structure with Scaffold-GS [18], our approach enables the simultaneous construction of Level-of-Detail (LOD) details and refinement of the scene representation during training, rather than deferring the generation of a compressed LOD model to later stages.

3. Method

In this section, we introduce **HUG**, a **Hierarchical Urban Gaussian Splatting** method designed for high-quality reconstruction and rendering of large-scale aerial urban scenes. An overview of the proposed method is illustrated in Section 2.1.

3.1. Preliminary: 3D Gaussian Splatting

3D Gaussian Splatting (3DGS) [11] represents a 3D scene using a set of anisotropic Gaussian primitives. Each Gaussian is defined by a mean position $\boldsymbol{\mu} \in \mathbb{R}^3$ and a covariance matrix $\boldsymbol{\Sigma} \in \mathbb{R}^{3 \times 3}$:

$$G(\boldsymbol{x}) = \exp\left(-\frac{1}{2}(\boldsymbol{x} - \boldsymbol{\mu})^\top \boldsymbol{\Sigma}^{-1}(\boldsymbol{x} - \boldsymbol{\mu})\right), \quad (1)$$

where $\boldsymbol{x} \in \mathbb{R}^3$ is a point in space. Each Gaussian also has an opacity $\alpha \in [0, 1]$ and color features for view-dependent rendering. To synthesize images, Gaussians are projected into the image space using camera parameters, producing 2D Gaussian representations:

$$G'(\boldsymbol{x}') = \exp\left(-\frac{1}{2}(\boldsymbol{x}' - \boldsymbol{\mu}')^\top \boldsymbol{\Sigma}'^{-1}(\boldsymbol{x}' - \boldsymbol{\mu}')\right), \quad (2)$$

where $\boldsymbol{x}' \in \mathbb{R}^2$ is a pixel position. The final image is rendered by compositing these projected Gaussians using alpha blending:

$$C(\boldsymbol{x}') = \sum_i T_i \alpha_i G'_i(\boldsymbol{x}') \boldsymbol{c}_i, \quad T_i = \prod_{j=1}^{i-1} (1 - \alpha_j G'_j(\boldsymbol{x}')), \quad (3)$$

with \boldsymbol{c}_i being the color of the i -th Gaussian. The rendering process is differentiable, allowing optimization of Gaussian parameters by minimizing the difference between rendered and ground truth images.

3.2. Visibility-based Partitioning

To reconstruct large-scale aerial urban scenes, the original 3DGS method must adopt a divide-and-conquer strategy due to memory limitations. We propose a simple yet efficient visibility-based partitioning strategy, which takes only 1 minute on the *MatrixCity* dataset, whereas CityGS [17] requires approximately 2 hours. Additionally, we integrate an SVM mask derived from visibility, enabling our method to focus more effectively on in-block regions, further enhancing reconstruction quality.

Scene Partitioning. Our partitioning approach leverages the sparse point cloud P generated by COLMAP [27] as the foundation. The scene is uniformly divided into multiple blocks indexed by j , ensuring controlled block sizes to prevent memory overflow. Therefore, the initial sparse point cloud for block j is $P_j \subseteq P$. Each block will be reconstructed independently, and can be processed in parallel across multiple GPUs and machines, allowing for efficient use of computational resources.

Visibility-Based View Partitioning. To determine the appropriate training views for block j , we compute the total number of reprojected visible sparse points of block j in image I_i . An image I_i is included in the training set \mathcal{T}_j for block j if the number of visible points exceeds a threshold τ_p :

$$I_i \in \mathcal{T}_j \quad \text{if} \quad \sum_{p \in P_j} \mathbb{I}(V(p, I_i)) > \tau_p \quad (4)$$

where $\mathbb{I}(V(p, I_i))$ is an indicator function that takes the value 1 if point $p \in P_j$ is visible in image I_i , and 0 otherwise. This selection criterion ensures that only images with sufficient visibility of block j contribute to its reconstruction, reducing redundancy while preserving critical information.

Visibility Mask Generation. For each image I_i and block j , we generate a visibility mask $M_i^j(u, v)$ to indicate which regions of the image correspond to block j . The mask is computed by reprojecting the sparse 3D points of block j into the image space, followed by non-linear classification to segment the visible region:

$$M_i^j(u, v) = \begin{cases} 1, & \text{if } (u, v) \text{ corresponds to block } j, \\ 0, & \text{otherwise,} \end{cases} \quad (5)$$

where (u, v) are pixel coordinates in image I_i .

The generated mask actively contributes to the training stage by concentrating on regions that provide key information for the target block, thereby reducing computational redundancy and enhancing reconstruction quality within the block.

3.3. Hierarchical Neural Gaussian

We employ an Octree-based hierarchical reconstruction strategy, leveraging neural Gaussians derived from Anchors to optimize each block. Built upon Scaffold-GS [18] and Octree-GS [26], our system has a combination of LOD and Neural Gaussian capabilities. To the best of our knowledge, we are the first to apply a combination of block-trained neural Gaussians and LOD techniques throughout the entire pipeline to the reconstruction and rendering of aerial urban scenes.

Hierarchical Anchor Initialization and Selection Our anchors are initialized at the centers of the nodes of an octree that covers the 3D space. The octree initialization for each block starts with a coarse 3D point cloud P_j corresponding to block j , while the complete point cloud P is typically obtained from COLMAP [27] or PixSfM [16]. Inspired by the Octree-GS [26], the maximum level of the octree K is determined by d_{max} and d_{min} , the 0.95 and 0.05

quantiles of the distances between all points in P_j and all the camera centers. It is calculated as follows:

$$K = \lfloor \log_2(d_{max}/d_{min}) \rfloor + 1 \quad (6)$$

where $\lfloor \cdot \rfloor$ denotes the rounding operation. Anchors with various levels of detail (LOD) are generated in an octree manner, placed at the nodes that contain any point from P_j . For each training view, the predicted level for each visible anchor is calculated as follows:

$$\hat{L} = \lfloor \min(\max(\log_2(d_{max}/d), 0), K - 1) \rfloor \quad (7)$$

where d is the distance between an anchor and the camera center. Only anchors with levels $L \leq \hat{L}$ are selected for further optimization. As shown by the red-marked portion in Figure 3.

Hierarchical Anchor Optimization The selected anchors are first decomposed into multiple neural Gaussians, which are then rendered using alpha blending as defined in Equation (3). The resulting image is optimized against the training data using an L1 color loss l_1 and an SSIM structure loss l_s , following a similar approach to 3DGS [11] and Octree-GS [26].

In our work, we observe that optimizing hierarchical neural Gaussians using the aforementioned strategy leads to obvious floaters and suboptimal outcomes, as illustrated in Figure 5. To resolve the problems above, a novel **hierarchical weighted image supervision** is introduced as shown by the green-marked portion of Figure 3.

We begin by rendering anchors with levels $L \leq \hat{L}$ according to Equation (7), the rendered image R_{full} is then compared with the ground truth image gt using the L1 loss l_1 and SSIM loss l_s , weighted by λ and $\gamma = 1 - \lambda$. Next, we render only the anchors with the finest level $K - 1$, and this rendered image R_{K-1} is evaluated with l_1 and l_s , but with weights $\lambda/2^K$ and $\gamma/2^1$, respectively. For anchors with levels equal to $K - 2$, the weights are $\lambda/2^{K-1}$ and $\gamma/2^2$. This process continues until level 0.

Our hierarchical weighted image supervision also incorporates an opacity mask m_L^o , which addresses the presence of extensive transparent regions that arise when rendering higher-level anchors, as shown by level 3 in Figure 3. Additionally, a weighting factor θ is introduced to balance this component against the traditional training content. Accordingly, the hierarchical loss in our framework can be formulated as follows:

$$l_{hier} = \lambda \cdot l_1(gt, R_{full}) + \gamma \cdot l_s(gt, R_{full}) + \theta \cdot \sum_{k=1}^K \left(\frac{\lambda}{2^{K+1-k}} \cdot l_1(gt, R_{K-k}, m_{K-k}^o) + \frac{\gamma}{2^k} \cdot l_s(gt, R_{K-k}, m_{K-k}^o) \right) \quad (8)$$

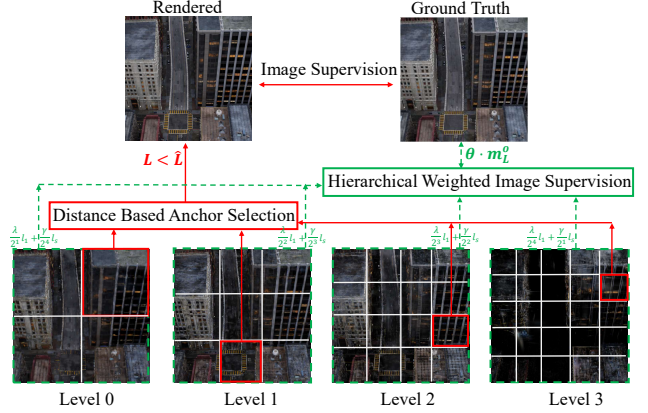


Figure 3. Hierarchical Octree Gaussian Training Strategy. We first select visible anchors based on the distance between the anchor and the camera center across all levels to render a complete scene image. Simultaneously, anchors from different levels are rendered separately, with distinct L1 and SSIM weights applied to evaluate the rendered image at each level.

This approach is designed to render higher-level anchors with greater detail, while lower-level anchors focus on capturing approximate colors to serve as a foundation for the fully rendered images. This novel hierarchical weighted image supervision ensures that all anchors remain active during training, enhancing hierarchical optimization and improving overall image quality. Our hierarchical anchor supervision strategy effectively addresses the issue of anomalous rendering in OctreeGS [26], as shown in Figure 5.

Anchor Splitting Splitting Gaussians or Anchors based on gradients, as proposed in 3DGS [11] and ScaffoldGS [18], involves dividing Gaussians with gradient values Δg exceeding a threshold τ_g into two new Gaussians with similar properties.

However, as training progresses, an increasing number of anchors tend to average the loss, causing the gradient threshold τ_g to become less effective. To address this, we propose an innovative **dynamic gradient threshold** strategy, where the gradient threshold for splitting is gradually decreased during training: $\tau_g(i) = \tau_g \cdot \eta^{\lfloor i/M \rfloor}$, where i is the current iteration number, M is the interval, and η is the decrease rate.

In the training process, we observed that some anchors have gradients significantly greater than the gradient threshold $\tau_g(i)$, indicating that these anchors are unsuitable for remaining in the current LOD. To address this, we propose an innovative **dynamic anchor level transition** strategy that

adaptively refines anchor levels as follow:

$$L = \min \left(K - 1, L + \left\lfloor \sum (0.01 \cdot \mathbb{I}(\Delta g > \beta \cdot \tau_g(i))) \right\rfloor \right) \quad (9)$$

where L is the initialized level of an anchor, β is a hyperparameter larger than 1, and \mathbb{I} is the indicator function that checks whether the anchor’s gradient at a given training iteration i surpasses β times the dynamic gradient threshold. Each time the condition is met, the anchor’s level L is gradually increased by 0.01.

This design allows anchors to dynamically adjust their levels based on local gradient magnitudes, ensuring higher-resolution details in regions where greater precision is needed. By progressively refining anchor levels, our approach enhances the adaptability of the hierarchical anchor representation, leading to improved reconstruction quality.

Anchor Pruning Pruning anchors or Gaussians based on opacity is a common technique. However, relying solely on opacity may lead to improper optimization of some anchors due to their LOD properties, as illustrated in Figure 5. Previous works [11, 18, 26] often overlooked Gaussians with low visibility counts during pruning.

In our work, we propose an innovative **visibility-based anchor pruning** strategy specially designed for hierarchical anchors. After every M iterations of training with only distance-based anchor selection, anchors with a visibility count lower than ϵ_c will also be pruned.

3.4. Scene Fusion and Rendering

Local Scene Refiltering After completing training in all blocks, previous works, such as CityGS [17], typically re-filter Gaussians whose center positions lie outside the block boundaries. However, we found that this approach can introduce artifacts near the boundaries. Specifically, even if an anchor’s center is outside the block, the neural Gaussians it generates often have centers that fall within the block.

To address this, we propose an innovative **greedy vote-based anchor refiltering** strategy. For any given anchor, it is retained if its center lies within the block. If the anchor’s center is outside the block but more than half of its generated neural Gaussians have centers within the block, the anchor is also preserved. Notably, our method follows a greedy approach, as it selectively retains anchors based on voting results but does not actively remove them.

Global Scene Rendering After refiltering, all blocks are stitched together. Methods like CityGS [17] can directly leverage the 3DGS [11] rasterization pipeline for global rendering. However, methods such as Octree-GS [26], which incorporate neural Gaussians, rely on small MLPs. These MLPs are trained separately for different neural networks

and thus have distinct weights, making Octree-GS unsuitable for direct application to multi-block scenes. To overcome this limitation, we reimplement the rasterization process to support the loading of multiple MLPs. During rendering, all visible anchors are first selected, and their corresponding neural Gaussians are then generated in parallel using the MLP trained on the respective block. This multi-MLP rendering strategy strikes a balance between leveraging the efficiency of MLPs and accommodating their limited learning capacity, enabling seamless rendering across blocks.

4. Experiments

4.1. Implementation Details

We built our method on the foundation of Octree-GS [26] for implementation. Our framework integrates innovative techniques, including visibility-based partitioning, hierarchical weighted image supervision, and a novel anchor splitting and pruning strategy. We modified the rendering code and the SIBR viewer [4] to support LOD rendering of neural Gaussians generated by multiple MLPs from different blocks, enabling real-time rendering of large-scale aerial urban scenes.

We first apply our proposed visibility-based partitioning method to divide the scene and views into multiple blocks. The point cloud threshold τ_p is setting as 800. We then perform block-wise scene optimization. The weights balancing components in the l_{hier} are set as $\lambda = 0.2$, $\gamma = 0.8$, and $\theta = 0.02$. For every $M = 5000$ iterations training, anchors with visibility count lower than $\epsilon_c = 5$ will be pruned, and gradient threshold $\epsilon_g = 2e^{-6}$ will be decreased by $\eta = 0.8$. The β in dynamic anchor level transition is set as 4. And the opacity mask m_L^o is obtained with pixels with opacity larger than 0.5. All experiments were conducted on a machine with 8 Nvidia A6000 48GB GPUs and 2 Intel Xeon 6330 CPUs.

4.2. Evaluation

We evaluated our method on five diverse scenes spanning different scales and environments. Our experiments included a synthetic *Small City* scene from the city-scale dataset *MatrixCity* [14], covering an area of 2.7 km^2 . Beyond synthetic data, we tested our approach on real-world datasets, including *Residence*, *Rubble*, *Building*, and *Sci-Art* from Mega-NeRF [33]. Following prior works [5, 17, 18, 26, 33, 36, 37], we downsampled the four real-world datasets by a factor of 4 and reduced the image resolution to 1.6k for *MatrixCity*.

For quantitative evaluation, we employed standard metrics: Peak Signal-to-Noise Ratio (**PSNR**), Structural Similarity Index Measure (**SSIM**), and Learned Perceptual Image Patch Similarity (**LPIPS**) [35].



Figure 4. Qualitative comparison with state-of-the-art methods on one synthetic and four real-world datasets. Red insets highlight patches that reveal notable visual differences between these methods.

We compared our method against several state-of-the-art baselines, including Mega-NeRF [33], 3DGS [11], CityGS [17], OctreeGS [26], VastGS [15], and Hier-GS [12]. More details on the settings for each method are provided in the supplement.

4.3. Results Analysis

Quantitative Comparisons Table 1 presents the quantitative results. Except for the PSNR metric in the *Sci-Art* scene, possibly due to the large number of distant views, where our results are lower than Mega-NeRF [33] but still outperform all GS-based methods. Across all other metrics, it surpasses all baseline methods. Notably, our method exceeds Octree-GS [26] by over 1.5 PSNR, demonstrating the effectiveness of our block-based recon-

struction and other proposed innovations. Additionally, we achieve superior performance compared to CityGS [29] and VastGS [15], further validating the effectiveness of our hierarchical representation combined with neural Gaussians. Our method also outperforms Hier-GS [12], which we attribute to our specific design tailored for large-scale aerial scenarios. These results further underscore the efficacy of our visibility-based partitioning strategy.

Qualitative Comparisons Figure 4 provides qualitative comparisons between our method and others across five diverse scenes. In the *MatrixCity* scene, our method excels at reconstructing intricate details, such as rooftop textures, facade steel structures, and street lamps, while preserving the fine structures with high fidelity. In the *Residence* scene,

	MatrixCity			Residence			Rubble			Building			Sci-Art		
Metrics	SSIM↑	PSNR↑	LPIPS↓	SSIM↑	PSNR↑	LPIPS↓	SSIM↑	PSNR↑	LPIPS↓	SSIM↑	PSNR↑	LPIPS↓	SSIM↑	PSNR↑	LPIPS↓
MegaNeRF [33]	-	-	-	0.628	22.08	0.489	0.553	24.06	0.516	0.547	20.93	0.504	0.770	25.60	0.390
3DGS [11]	0.735	23.67	0.384	0.791	21.44	0.236	0.777	25.47	0.277	0.720	20.46	0.305	0.830	21.05	0.242
Octree-GS [26]	0.814	26.41	0.282	-	-	-	-	-	-	-	-	-	-	-	-
Hier-GS [12]	0.842	26.67	0.251	0.776	20.24	0.221	0.765	22.28	0.257	0.733	20.04	0.262	0.828	19.74	0.207
VastGS [15]	-	-	-	0.777	20.38	0.247	0.766	25.10	0.294	0.740	21.69	0.293	0.809	21.66	0.269
CityGS [17]	0.865	27.46	0.204	0.813	22.00	0.211	0.813	25.77	0.228	0.778	21.55	0.246	0.837	21.39	0.230
Ours	0.883	28.02	0.142	0.813	22.33	0.207	0.839	26.42	0.197	0.792	22.35	0.228	0.846	21.83	0.204

Table 1. Quantitative comparison of our method with state-of-the-art methods. The best scores in each column are highlighted with red background, second best with orange, and third best with yellow. The symbol ‘-’ denotes experiments that are difficult to reproduce.

our approach captures the truck’s details more thoroughly than the baseline methods. In the *Rubble* scene, while all methods successfully reconstruct the red object, our method stands out by exhibiting fewer artifacts in the surrounding rubble piles. In the *Building* scene, both our method and Hier-GS [12] reconstruct the staircase steps accurately, but Hier-GS [12] suffers from noticeable color deviations. Finally, in the *Sci-Art* scene, our method successfully recovers a building nestled between two background structures, which other methods fail to reconstruct entirely.

Figure 5 also illustrates how our method effectively eliminates the unoptimized anchor issue in Octree-GS [26], which often becomes apparent when zooming in on the scene.

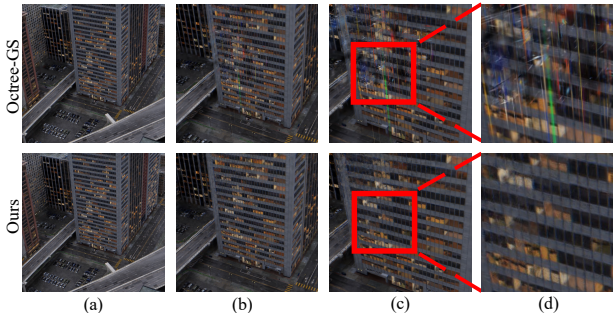


Figure 5. The unoptimized anchor issue of Octree-GS [26]. (a). A training view. (b). As the perspective zooms in, multicolored artifacts begin to appear in Octree-GS [26]. (c). Further zooming amplifies these artifacts, whereas our method effectively eliminates them. (d). Close-up view of the issue.

Partitioning and Optimization Efficiency Partitioning large-scale scenes into smaller blocks followed by optimization has become a standard practice. Since these two stages are executed sequentially, the time consumption of each directly impacts the overall performance. Table 2 presents the time consumption of our method compared to related approaches. Our visibility-based partitioning is both simple and efficient, consistently completing in about one

Scene	MatrixCity		Rubble		Residence		Building		Sci-Art	
	Part.	Opt.	Part.	Opt.	Part.	Opt.	Part.	Opt.	Part.	Opt.
CityGS [17]	188	61	77	51	118	79	97	78	71	55
VastGS [15]	51	89	4	44	10	59	8	68	20	52
Hier-GS [12]	9.8	119	12.7	101	8.0	137	4.4	130	7.6	120
Ours	1	67	<1	52	<1	78	<1	63	<1	59

Table 2. Partitioning and optimization efficiency of different methods across various scenes, with time measured in minutes.

minute, whereas CityGS [17] requires over two hours for the *MatrixCity* dataset. Efficient optimization within each block is equally crucial. While most methods, including ours, maintain an optimization time of approximately one hour per block, Hier-GS [12] takes nearly two hours due to additional post-processing refinements applied to each block.

Model Setting	SSIM ↑	PSNR ↑	LPIPS ↓
Baseline	0.747	25.06	0.281
add C1	0.779	25.40	0.244
add C2	0.807	25.74	0.229
add C3	0.834	26.33	0.201
Full model	0.839	26.42	0.197

Table 3. Ablation results on *Rubble* scene.

Ablation To comprehensively assess the impact of each component in our proposed method, we conducted an ablation study on the *Rubble* scene. Specifically, we evaluate the effectiveness of our approach by progressively incorporating key components: visibility-based masking (C1), hierarchical weighted image supervision (C2), dynamic gradient thresholding (C3), and finally, our full model. Table 3 presents the corresponding results, demonstrating the effectiveness of our proposed strategies.

5. Conclusion

In this paper, we present **HUG**, a novel Hierarchical Urban Gaussian Splatting method designed to reconstruct and render large-scale aerial urban scenes with high quality.

Comprehensive experimental results demonstrating State-of-the-Art performance of our model, proves the effectiveness of our proposed visibility-based partitioning, hierarchical weighted image supervision, dynamic gradient threshold, and other proposals.

Despite our approach’s advantages, a few limitations should be addressed in future work. First, our method does not account for dynamic objects. This can be improved by incorporating lighting decoupling and appearance encoding. Second, the data partitioning process relies on the sparse point cloud generated by COLMAP [27], which may lead to issues in low-texture areas. Combining pose-free Gaussian methods [10] may help it. Finally, our method does not support integrated aerial-ground training and rendering. This functionality could be incorporated in future research to enable more comprehensive scene reconstruction.

References

- [1] Sameer Agarwal, Yasutaka Furukawa, Noah Snavely, Ian Simon, Brian Curless, Steven M Seitz, and Richard Szeliski. Building rome in a day. *Communications of the ACM*, 54(10):105–112, 2011. 3
- [2] Jonathan T Barron, Ben Mildenhall, Matthew Tancik, Peter Hedman, Ricardo Martin-Brualla, and Pratul P Srinivasan. Mip-nerf: A multiscale representation for anti-aliasing neural radiance fields. In *Proceedings of the IEEE/CVF International Conference on Computer Vision*, pages 5855–5864, 2021. 2, 3
- [3] Jonathan T. Barron, Ben Mildenhall, Dor Verbin, Pratul P. Srinivasan, and Peter Hedman. Mip-nerf 360: Unbounded anti-aliased neural radiance fields. *CVPR*, 2022. 2
- [4] Sebastien Bonopera, Jerome Esnault, Siddhant Prakash, Simon Rodriguez, Theo Thonat, Mehdi Benadel, Gaurav Chaurasia, Julien Philip, and George Drettakis. sibr: A system for image based rendering, 2020. 6
- [5] Junyi Chen, Weicai Ye, Yifan Wang, Danpeng Chen, Di Huang, Wanli Ouyang, Guofeng Zhang, Yu Qiao, and Tong He. Gigags: Scaling up planar-based 3d gaussians for large scene surface reconstruction, 2024. 3, 6
- [6] Jiadi Cui, Junming Cao, Yuhui Zhong, Liao Wang, Fuqiang Zhao, Penghao Wang, Yifan Chen, Zhipeng He, Lan Xu, Yujiao Shi, et al. Letsgo: Large-scale garage modeling and rendering via lidar-assisted gaussian primitives. *arXiv preprint arXiv:2404.09748*, 2024. 3
- [7] Zhiwen Fan, Kevin Wang, Kairun Wen, Zehao Zhu, De-ji Xu, and Zhangyang Wang. Lightgaussian: Unbounded 3d gaussian compression with 15x reduction and 200+ fps. *arXiv preprint arXiv:2311.17245*, 2023. 2
- [8] Sara Fridovich-Keil, Alex Yu, Matthew Tancik, Qinlong Chen, Benjamin Recht, and Angjoo Kanazawa. Plenoxels: Radiance fields without neural networks. In *Proceedings of the IEEE/CVF Conference on Computer Vision and Pattern Recognition*, pages 5501–5510, 2022. 2
- [9] Christian Früh and Avideh Zakhor. An automated method for large-scale, ground-based city model acquisition. *International Journal of Computer Vision*, 60:5–24, 2004. 2
- [10] Sunghwan Hong, Jaewoo Jung, Heeseong Shin, Jisang Han, Jiaolong Yang, Chong Luo, and Seungryong Kim. Pf3plat: Pose-free feed-forward 3d gaussian splatting. *arXiv preprint arXiv:2410.22128*, 2024. 9
- [11] Bernhard Kerbl, Georgios Kopanas, Thomas Leimkühler, and George Drettakis. 3d gaussian splatting for real-time radiance field rendering. *ACM Transactions on Graphics*, 42(4), 2023. 2, 4, 5, 6, 7, 8, 1
- [12] Bernhard Kerbl, Andreas Meuleman, Georgios Kopanas, Michael Wimmer, Alexandre Lanvin, and George Drettakis. A hierarchical 3d gaussian representation for real-time rendering of very large datasets. *ACM Transactions on Graphics (TOG)*, 43(4):1–15, 2024. 7, 8, 1
- [13] Xiaowei Li, Changchang Wu, Christopher Zach, Svetlana Lazebnik, and Jan-Michael Frahm. Modeling and recognition of landmark image collections using iconic scene graphs. In *Computer Vision—ECCV 2008: 10th European Conference on Computer Vision, Marseille, France, October 12–18, 2008, Proceedings, Part I 10*, pages 427–440. Springer, 2008. 2
- [14] Yixuan Li, Lihan Jiang, Linning Xu, Yuanbo Xiangli, Zhenzhi Wang, Dahua Lin, and Bo Dai. Matrixcity: A large-scale city dataset for city-scale neural rendering and beyond. In *Proceedings of the IEEE/CVF International Conference on Computer Vision*, pages 3205–3215, 2023. 6
- [15] Jiaqi Lin, Zhihao Li, Xiao Tang, Jianzhuang Liu, Shiyong Liu, Jiayue Liu, Yangdi Lu, Xiaofei Wu, Songcen Xu, Youliang Yan, and Wenming Yang. Vastgaussian: Vast 3d gaussians for large scene reconstruction. In *CVPR*, 2024. 3, 7, 8, 1
- [16] Philipp Lindenberger, Paul-Edouard Sarlin, Viktor Larsson, and Marc Pollefeys. Pixel-Perfect Structure-from-Motion with Featuremetric Refinement. In *ICCV*, 2021. 4
- [17] Yang Liu, He Guan, Chuanchen Luo, Lue Fan, Naiyan Wang, Junran Peng, and Zhaoxiang Zhang. Citygaussian: Real-time high-quality large-scale scene rendering with gaussians. 2024. 1, 3, 4, 6, 7, 8
- [18] Tao Lu, Mulin Yu, Linning Xu, Yuanbo Xiangli, Limin Wang, Dahua Lin, and Bo Dai. Scaffold-gs: Structured 3d gaussians for view-adaptive rendering. *arXiv preprint arXiv:2312.00109*, 2023. 2, 3, 4, 5, 6
- [19] Ricardo Martin-Brualla, Noha Radwan, Mehdi SM Sajjadi, Jonathan T Barron, Alexey Dosovitskiy, and Daniel Duckworth. Nerf in the wild: Neural radiance fields for unconstrained photo collections. In *Proceedings of the IEEE/CVF Conference on Computer Vision and Pattern Recognition*, pages 7210–7219, 2021. 2
- [20] Ben Mildenhall, Pratul P Srinivasan, Matthew Tancik, Jonathan T Barron, Ravi Ramamoorthi, and Ren Ng. Nerf: Representing scenes as neural radiance fields for view synthesis. *Communications of the ACM*, 65(1):99–106, 2021. 1, 2, 3
- [21] Wieland Morgenstern, Florian Barthel, Anna Hilsmann, and Peter Eisert. Compact 3d scene representation via self-organizing gaussian grids. *arXiv preprint arXiv:2312.13299*, 2023. 2

- [22] Thomas Müller, Alex Evans, Christoph Schied, and Alexander Keller. Instant neural graphics primitives with a multiresolution hash encoding. *ACM Transactions on Graphics (TOG)*, 41(4):1–15, 2022. 2
- [23] Marc Pollefeys, David Nistér, J-M Frahm, Amir Akbarzadeh, Philippos Mordohai, Brian Clipp, Chris Engels, David Gallup, S-J Kim, Paul Merrell, et al. Detailed real-time urban 3d reconstruction from video. *International Journal of Computer Vision*, 78:143–167, 2008. 2
- [24] Albert Pumarola, Enric Corona, Gerard Pons-Moll, and Francesc Moreno-Noguer. D-nerf: Neural radiance fields for dynamic scenes. In *Proceedings of the IEEE/CVF Conference on Computer Vision and Pattern Recognition*, pages 10318–10327, 2021. 2
- [25] Christian Reiser, Rick Szeliski, Dor Verbin, Pratul Srinivasan, Ben Mildenhall, Andreas Geiger, Jon Barron, and Peter Hedman. Merf: Memory-efficient radiance fields for real-time view synthesis in unbounded scenes. *ACM Transactions on Graphics (TOG)*, 42(4):1–12, 2023. 2
- [26] Kerui Ren, Lihan Jiang, Tao Lu, Mulin Yu, Linning Xu, Zhangkai Ni, and Bo Dai. Octree-gs: Towards consistent real-time rendering with lod-structured 3d gaussians, 2024. 3, 4, 5, 6, 7, 8, 1
- [27] Johannes Lutz Schönberger and Jan-Michael Frahm. Structure-from-motion revisited. In *Conference on Computer Vision and Pattern Recognition (CVPR)*, 2016. 3, 4, 9
- [28] Noah Snavely, Steven M Seitz, and Richard Szeliski. Photo tourism: exploring photo collections in 3d. In *ACM siggraph 2006 papers*, pages 835–846. 2006. 3
- [29] Kaiwen Song and Juyong Zhang. City-on-web: Real-time neural rendering of large-scale scenes on the web. *arXiv preprint arXiv:2312.16457*, 2023. 7
- [30] Towaki Takikawa, Joey Litalien, Kangxue Yin, Karsten Kreis, Charles Loop, Derek Nowrouzezahrai, Alec Jacobson, Morgan McGuire, and Sanja Fidler. Neural geometric level of detail: Real-time rendering with implicit 3d shapes. In *Proceedings of the IEEE/CVF Conference on Computer Vision and Pattern Recognition*, pages 11358–11367, 2021. 3
- [31] Matthew Tancik, Vincent Casser, Xinchun Yan, Sabeek Pradhan, Ben Mildenhall, Pratul P Srinivasan, Jonathan T Barron, and Henrik Kretzschmar. Block-nerf: Scalable large scene neural view synthesis. In *Proceedings of the IEEE/CVF Conference on Computer Vision and Pattern Recognition*, pages 8248–8258, 2022. 3
- [32] Matthew Tancik, Ethan Weber, Evonne Ng, Ruilong Li, Brent Yi, Terrance Wang, Alexander Kristoffersen, Jake Austin, Kamyar Salahi, Abhik Ahuja, et al. Nerfstudio: A modular framework for neural radiance field development. In *ACM SIGGRAPH 2023 Conference Proceedings*, pages 1–12, 2023. 2
- [33] Haithem Turki, Deva Ramanan, and Mahadev Satyanarayanan. Mega-nerf: Scalable construction of large-scale nerfs for virtual fly-throughs. In *Proceedings of the IEEE/CVF Conference on Computer Vision and Pattern Recognition*, pages 12922–12931, 2022. 3, 6, 7, 8, 1
- [34] Dejia Xu, Yifan Jiang, Peihao Wang, Zhiwen Fan, Humphrey Shi, and Zhangyang Wang. Sinnerf: Training neural radiance fields on complex scenes from a single image. In *European Conference on Computer Vision*, pages 736–753. Springer, 2022. 2
- [35] Richard Zhang, Phillip Isola, Alexei A Efros, Eli Shechtman, and Oliver Wang. The unreasonable effectiveness of deep features as a perceptual metric. In *Proceedings of the IEEE conference on computer vision and pattern recognition*, pages 586–595, 2018. 6
- [36] Yuqi Zhang, Guanying Chen, and Shuguang Cui. Efficient large-scale scene representation with a hybrid of high-resolution grid and plane features. *arXiv preprint arXiv:2303.03003*, 2023. 6
- [37] MI Zhenxing and Dan Xu. Switch-nerf: Learning scene decomposition with mixture of experts for large-scale neural radiance fields. In *The Eleventh International Conference on Learning Representations*, 2022. 6

HUG: Hierarchical Urban Gaussian Splatting with Block-Based Reconstruction for Large-Scale Aerial Scenes

Supplementary Material

We provide a more detailed discussion on the settings of the compared methods, view partition results, and additional qualitative comparisons. A rendered video is also included for a more comprehensive comparison.

6. Settings of Compared Methods

We compared our method against several state-of-the-art baselines, including Mega-NeRF [33], 3DGS [11], CityGS [17], OctreeGS [26], VastGS [15], and Hier-GS [12]. The quantitative results for Mega-NeRF [33], 3DGS [11], and CityGS [17] are taken from the CityGS [17] paper. The quantitative results for OctreeGS [26] are sourced from the OctreeGS [26] paper. The results for Hier-GS [12] were obtained using the released source code with all default settings. The results for VastGS [15] are derived from the unofficial code available at <https://github.com/kangpeilun/VastGaussian>, with the same block number as CityGS [17] and ours. The qualitative results for CityGS [17] were obtained from the checkpoint provided by the authors.

7. Data Partitioning Results

To associate all training images with their respective blocks, we compute the total number of visible sparse points in each view. A threshold of $\tau_p = 800$ is then applied to determine the assignment of each training image to specific blocks. In CityGS [17], a coarse global 3DGS [11] model must first be constructed, followed by multiple renderings of all images corresponding to the number of blocks. VastGS [15] introduces a more complex camera selection strategy, incorporating position-based data selection, visibility-based camera selection, and coverage-based point selection, resulting in a significantly higher number of assigned cameras per block. VastGS [15] has an average of over 1,000 views per block on the MatrixCity dataset, which exceeds GPU memory limits for a single block. This is why we do not report its numerical results on this scene. For visual comparisons, we avoid that specific block whenever possible. In contrast, our data partitioning strategy assigns fewer images to each block, reducing memory consumption during training and allowing more computational resources to be dedicated to refining the in-block reconstruction. Figure 6 visualizes the number of training images per block, illustrating that our method allocates fewer images on average while still achieving superior rendering performance, as demonstrated in Table 1.

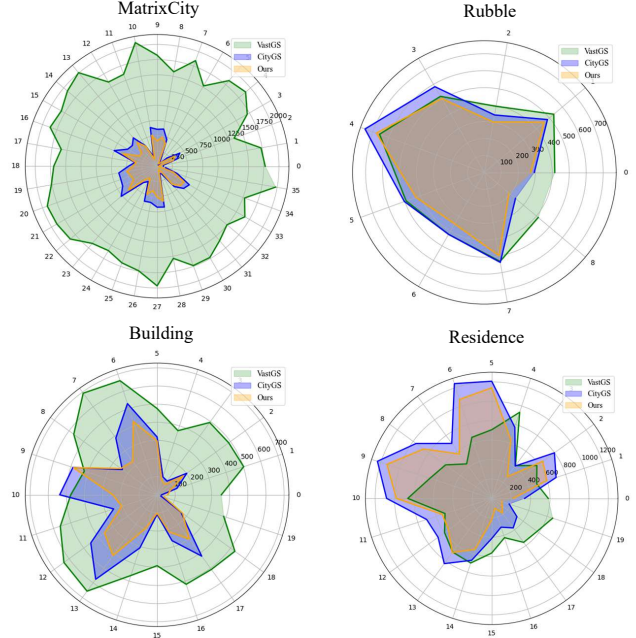


Figure 6. Comparison of view partition results among our method, VastGS [15], and CityGS [17] across four datasets. The radial coordinate indicates the number of training images assigned to each block, with each vertex representing a specific block. As shown, our method consistently assigns fewer images on average, demonstrating a more efficient partition strategy.

8. More Qualitative Comparisons

We provide additional qualitative comparisons in Figure 7 and Figure 8.

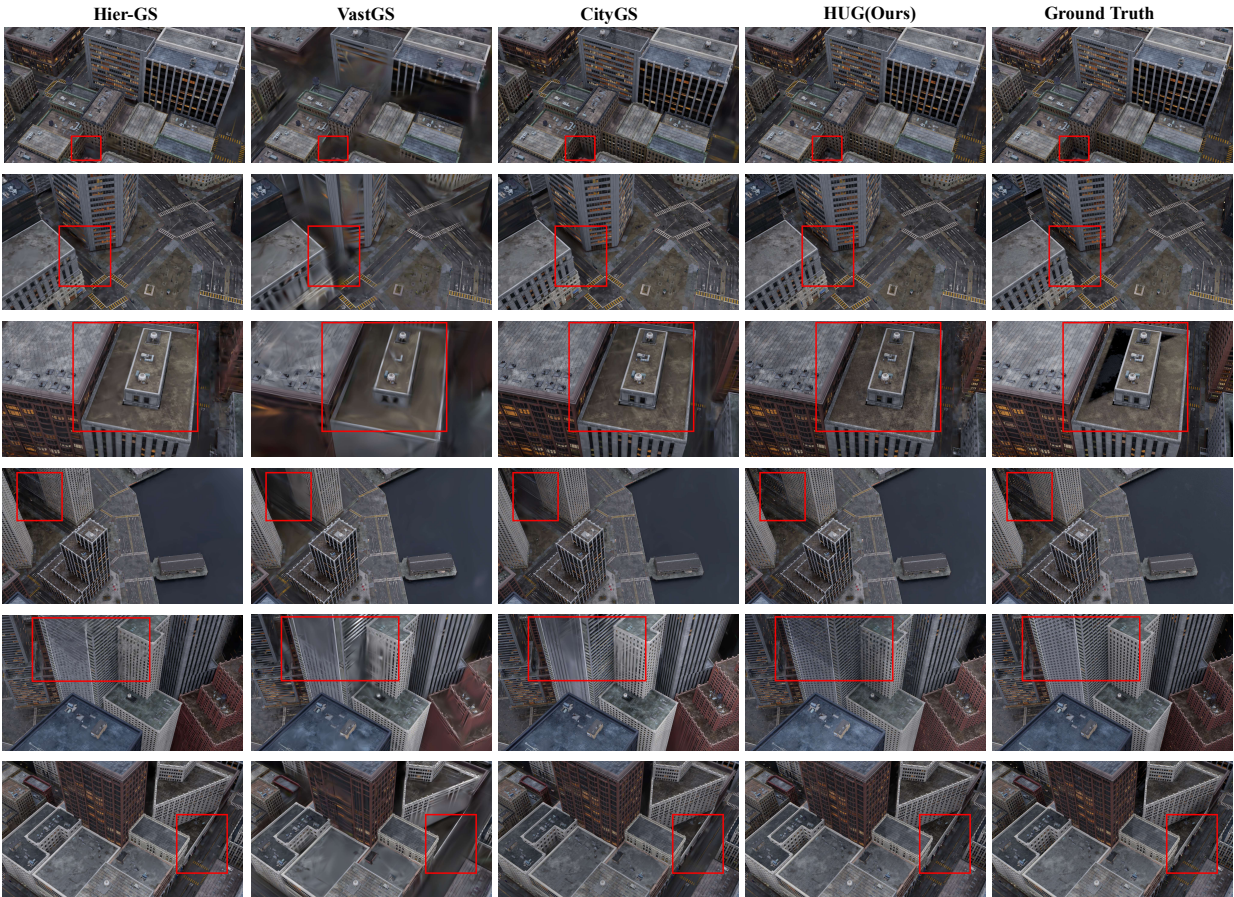


Figure 7. More qualitative comparisons on *MatrixCity* dataset.

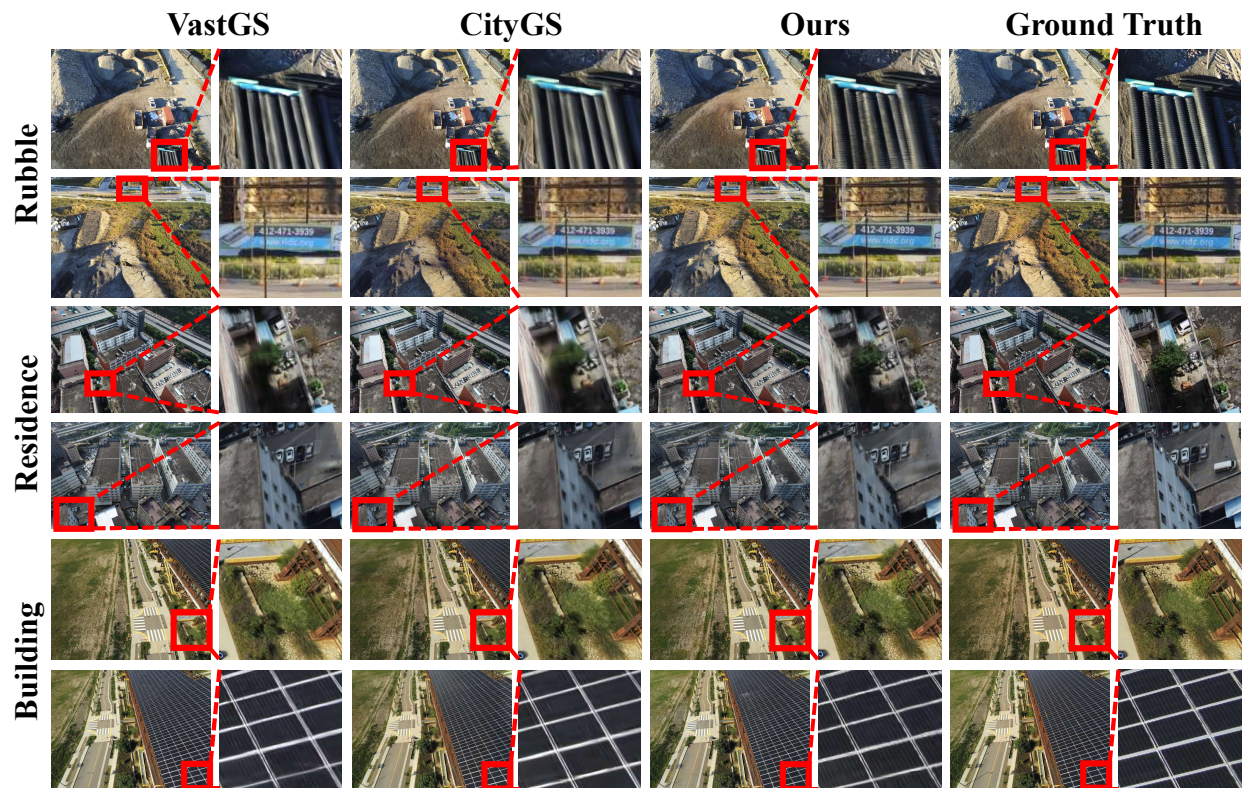


Figure 8. More qualitative comparisons on *Rubble*, *Residence* and *Building* datasets.